fibers

MDPI

Article

Melt-Spun, Cross-Section Modified Polycaprolactone Fibers for Use in Tendon and Ligament Tissue Engineering

Benedict Bauer [1,*], Caroline Emonts [1], Louisa Bonten [1], Rokaya Annan [1], Felix Merkord [1], Thomas Vad [1], Akram Idrissi [1], Thomas Gries [1] and Andreas Blaeser [2,3,*]

[1] Institut für Textiltechnik (ITA), RWTH Aachen University, 52074 Aachen, Germany; caroline.emonts@ita.rwth-aachen.de (C.E.); louisa.bonten@rwth-aachen.de (L.B.); r.annan@hotmail.de (R.A.); felix.merkord@ita.rwth-aachen.de (F.M.); thomas.vad@ita.rwth-aachen.de (T.V.); akram.idrissi@ita.rwth-aachen.de (A.I.); thomas.gries@ita.rwth-aachen.de (T.G.)

[2] Institute for BioMedical Printing Technology, Technical University of Darmstadt, 64289 Darmstadt, Germany

[3] Centre for Synthetic Biology, Technical University of Darmstadt, 64289 Darmstadt, Germany

* Correspondence: benedict.bauer@ita.rwth-aachen.de (B.B.); blaeser@idd.tu-darmstadt.de (A.B.); Tel.: +49-80-241-23476 (A.B.)

Abstract: Tissue Engineering is considered a promising route to address existing deficits of autografts and permanent synthetic prostheses for tendons and ligaments. However, the requirements placed on the scaffold material are manifold and include mechanical, biological and degradation-related aspects. In addition, scalable processes and FDA-approved materials should be applied to ensure the transfer into clinical practice. To accommodate these aspects, this work focuses on the high-scale fabrication of high-strength and highly oriented polycaprolactone (PCL) fibers with adjustable cross-sectional geometry and degradation kinetics applying melt spinning technology. Four different fiber cross-sections were investigated to account for potential functionalization and cell growth guidance. Mechanical properties and crystallinity were studied for a 24-week exposure to phosphate-buffered saline (PBS) at 37 °C. PCL fibers were further processed into scaffolds using multistage circular braiding with three different hierarchical structures. One structure was selected based on its morphology and scaled up in thickness to match the requirements for a human anterior cruciate ligament (ACL) replacement. Applying a broad range of draw ratios (up to DR9.25), high-strength PCL fibers with excellent tensile strength (up to 69 cN/tex) could be readily fabricated. The strength retention after 24 weeks in PBS at 37 °C was 83–93%. The following braiding procedure did not affect the scaffolds' mechanical properties as long as the number of filaments and the braiding angle remained constant. Up-scaled PCL scaffolds resisted loads of up to 4353.88 ± 37.30 N, whilst matching the stiffness of the human ACL (111–396 N/mm). In conclusion, this work demonstrates the fabrication of highly oriented PCL fibers with excellent mechanical properties. The created fibers represent a promising building block that can be further processed into versatile textile implants for tissue engineering and regenerative medicine.

Keywords: tissue engineering; ligament; tendon; polycaprolactone; PCL; melt spinning; cross-section modification; non-circular fibers; circular braiding; ACL

check for updates

Citation: Bauer, B.; Emonts, C.; Bonten, L.; Annan, R.; Merkord, F.; Vad, T.; Idrissi, A.; Gries, T.; Blaeser, A. Melt-Spun, Cross-Section Modified Polycaprolactone Fibers for Use in Tendon and Ligament Tissue Engineering. *Fibers* **2022**, *10*, 23. https://doi.org/10.3390/fib10030023

Academic Editor: Carlo Santulli

Received: 20 December 2021
Accepted: 1 March 2022
Published: 2 March 2022

Publisher's Note: MDPI stays neutral with regard to jurisdictional claims in published maps and institutional affiliations.

Copyright: © 2022 by the authors. Licensee MDPI, Basel, Switzerland. This article is an open access article distributed under the terms and conditions of the Creative Commons Attribution (CC BY) license (https://creativecommons.org/licenses/by/4.0/).

1. Introduction

Injuries of tendons and ligaments are responsible for individual morbidity, work loss and high costs for the health care system [1,2]. Current treatments include biological replacements in form of autografts or allografts. These show certain critical deficits, such as limited tissue availability, donor-site morbidity, tissue rejection and disease transmission. Alternative synthetic prostheses exhibit insufficient mechanical long-term durability [3]. Tissue Engineering is a promising alternative to combine the short-term advantages of prosthetic devices while avoiding long-term deficits [4–6]. However, high and yet unmet requirements are imposed on the material [6–8]. These include mechanical, biological and

degradation kinetics requirements: controllable degradation, biocompatibility, sufficient mechanical properties and maintenance during tissue regeneration, biofunctionality and processability [6,7,9–13].

Previous approaches in tissue engineering can be divided into two categories concerning the materials used: synthetic, degradable polyesters and natural polymers. Degradable polyesters such as polylactide acid (PLA), polyglycolide acid (PGA) and their copolymer polylactide-co-glycolide acid (PLGA) are easy, reproducible and available in large quantities and have good primary stability compared to most natural polymers. The acidic degradation products of PLA, PGA and PLGA can lead to inflammatory reactions, especially in tissues with low vascularization, such as ligaments and tendons [10,14,15]. It has been reported that implanted polylactid-based materials did not match the necessary mechanical long-term stability [4,16,17]. Natural polymers such as collagen provide excellent biocompatibility and biofunctionality. The limitations lie in the processability, batch dependency and mechanical properties (apart from silk). Altman et al. reported braided silk scaffolds that exhibited mechanical properties similar to those of the human anterior cruciate ligament (ACL) [9]. However, the major drawbacks, besides the cost of silk, are the immunogenic sericin proteins, the removal of which significantly alters the biomechanical properties [18]. Therefore, it is stated that the ideal material has not yet been found [7,8,19–21]. Due to the shortcomings of existing solutions, poly-ε-caprolactone (PCL) is considered a promising scaffold material in this study. PCL is also an aliphatic polyester for which no adverse effects due to acidic degradation products have been reported. It is FDA-approved for use as a co-polymer or coating for degradable surgical sutures (PCL®) to improve biocompatibility or reduce the embrittlement of PLLA during the degradation process [6,22–24]. PCL is used as a material for tissue engineering of tendons, bone and cartilage in form of nanofibers, foams and 3D printed structures [22]. Existing strategies for tendon and ligament scaffolds are manifold, including numerous studies on nanofibrous and yarn-based structures [25–32]. Given the high mechanical demands associated with tendons and ligaments, textile structures are considered promising to replace anisotropic tissues [26,33]. Textile technology offers an approach to the reproducible and scalable fabrication of high-strength, load-efficient 3D-scaffolds with adjustable and interconnected pores. Textile fabrication methods which are established for decades can be used based on melt-spun or solution-spun fibers [33–35]. In course of this, yarn-based tendon and ligament scaffolds have been produced primarily via braiding [11,20,36–41], braid-twisting [37,42–44], knitting [45–47], weaving [13,48–50] and embroidery [15,51,52]. For PCL in melt-spun form, however, there have been few reports in which it was used as a scaffold material for tendons or ligaments [53]. This is mainly due to the very slow degradation rate of PCL. However, in cases where long-term mechanical properties are required (e.g., tendon and ligament scaffolds), the slow degradation rate can be advantageous. For example, Sahoo et al. examined a knitted PLGA scaffold during hydrolytic degradation. The scaffold lost about 88% of its strength after 14 days [17]. Lam et al. studied the material degradation of PCL extensively and report that PCL can maintain its mechanical properties in vivo for more than 6 months [54]. Leroux et al. have performed a long-term in vitro degradation study of PCL fibers for 120 weeks, detecting only minor changes in the pH value and molecular weight during the initial 6 months [55]. In many cases, PCL is characterized by insufficient tensile strength and excessive elongation (such as 23 MPa and >700%, respectively) [24,56–58]. This, however, refers to unoriented PCL fibers. Mochuzuki et al. show that melt-spun PCL fibers can be produced with an excellent tensile strength of up to 7.15 g/den (~63 cN/tex; 769 MPa) at a 20.9% elongation [59,60]. In 2019, Leroux et al. reported the use of knotted PCL monofilament bundles for the replacement of rat ACL, indicating that PCL is a promising material for ligament tissue engineering with regard to tissue anchoring and inflammation, especially when it is improved with a surface functionalization [61]. However, to our knowledge there has been no study on mechanically potent PCL scaffolds for the human ACL yet. For this reason, the present study focusses on the mechanical evaluation and the potential for upscaling of PCL-based scaffolds with

respect to the necessary primary stability for use as human ACL, which is reported to be up to 2160 N at a cross-sectional area of 57.5 ± 16.2 mm^2 [33,62]. The stress at the failure values ranges between 13.7 and 36.4 MPa [6,63]. The focus was placed on braided scaffolds, as these can mimic the natural hierarchical structure of ligaments and are particularly suitable for high tensile loads in the axial direction. Furthermore, the mechanical properties and the morphological properties can be tailored by the design of the braided structure [34,64]. Therefore, three different designs to form a hierarchical braided structure using the same number of filaments were investigated. The effect of upscaling the number of filaments was consequently studied for one selected braided structure. Moreover, the aspect of the fibers' strength retention during exposure to PBS at 37 °C is investigated for four different fiber cross-sections, which can be utilized in future studies as a means for growth guidance or surface-driven functionalization.

2. Materials and Methods

2.1. Fiber Fabrication

Poly-ε-caprolactone pellets with a molecular weight of 80,000 Da (CAPA 6800®) were kindly provided by Perstorp Holding AB, Malmö, Sweden. Monofilaments and multifilaments were fabricated from PCL via melt spinning (Fourné Polymertechnik GmbH, Alfter, Germany). The PCL pellets were not dried prior to spinning. Extrusion temperatures (T_E) of T_E = 185–235 °C were used. Monofilaments and multifilaments were spun using circular as well as snowflake-shaped capillaries, the latter being an exemplary radial symmetric shape with a pronounced profile. The multifilament spinnerets exhibited ten capillaries. The spinning line was set up as indicated in Figure 1, comprising two godet pairs (for draw ratios >8.1 three godet pairs were used) as well as a winder (SAHM 260XE, Georg Sahm GmbH & Co. KG, Eschwege, Germany). The cooling of the polymer melt was achieved using a water bath for monofilaments and a blow chamber for multifilaments, respectively. Spin finish (Limanol LB25, Schill + Seilacher GmbH, Böblingen, Germany) was used in multifilament fabrication with a concentration of 10 vol% in deionized water.

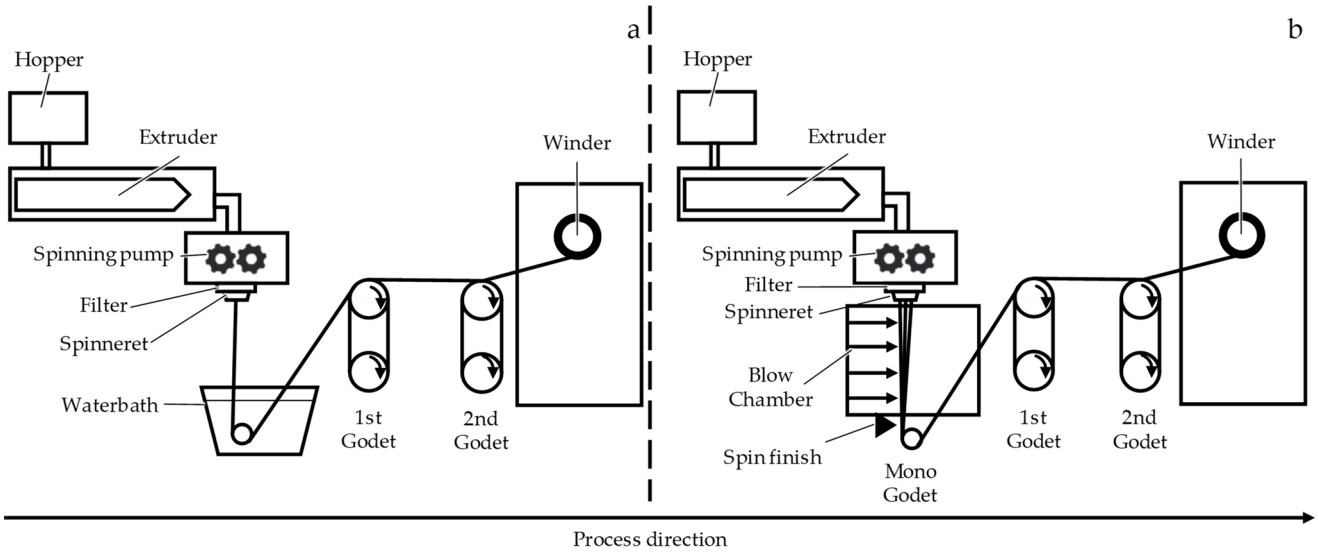

Figure 1. Process schematics of (**a**) monofilament and (**b**) multifilament spinning.

2.2. Braiding

Three-layered braids were fabricated from n_F = 96 (number of filaments) previously produced PCL monofilaments using a circular braiding machine (Steeger GmbH & Co. KG, Wuppertal, Germany–Type HS80/48). Within the braiding process, the filament-tension F_T was set to ~1 N using fine-wire bobbins (three deflection rollers) by Steeger. A process braiding angle of α_B = 13° was used for all braided structures. The rotation speed was set to 30 rpm. Three different braided structures were initially fabricated. "Sandwich A" was produced by overbraiding. The first layer was manufactured with the machine fully equipped with 48 filaments. The second and third layer had 24 filaments. "Braided Braid" is composed of four braided strands, each containing 24 filaments. In a second step, a braid is formed out of the four strands. The structure "Combination" consists of four braided strands with twelve filaments each. These were then braided and in a third step overbraided with 48 filaments. One of the structures (Sandwich A) was selected for an upscaling to human ACL dimensions. In the meantime, braided ligaments consisting of n_F = 192, 288 and 384 filaments were produced by adding layers of 48 filaments, respectively.

2.3. Mechanical Characterization

The yarn count was determined according to DIN EN 13392. Uniaxial tensile tests for fibers were performed in accordance with DIN EN ISO 2062. The braids were fixated at the ends with resin (Araldite® 2011, Huntsman, The woodlands, TX, USA) and carton to prevent slipping during tensile tests. The resin hardened 24 h at room temperature. Uniaxial tensile tests were then conducted in accordance with NF S 94-167-2 using a universal tensile testing device (Z100, ZwickRoell, Ulm, Germany). The geometry of the braided structures was measured manually using a digital caliper while the sample was preloaded with 2 N. The diameter was measured for each specimen at two positions in an orthogonal direction, respectively, to calculate the cross-sectional area.

2.4. Microscopic Analysis

The fiber cross-sections were investigated optically using a microscope (DM4000M, Leica Camera AG, Wetzlar, Germany). The "reference diameter" was calculated for all fiber morphologies based on the cross-sectional area, which was converted to the diameter of a perfectly circular cross-section. The cross-sectional area was derived from microscopic images using the software ImageJ. Prior to the scanning electron microscopy (SEM), the samples were coated with a thin layer of gold using a sputter coater. SEM was conducted using the secondary electron mode (JEOL JSM 6400; JEOL Ltd., Tokyo, Japan).

2.5. Differential Scanning Calorimetry (DSC)

Differential scanning calorimetry was performed under N_2 using a heat flux system (DSC 1, Mettler Toledo, Greifswald, Germany). The heating rate was 10 K/min. Crystallinity was calculated with the measured enthalpy of the first heating in reference to the enthalpy of entirely crystalline PCL (136 J/g). [58]

2.6. Wide-Angle X-ray Diffraction (WAXD)

The influence of the draw ratio on the orientation of the orthorhombic PCL crystallites in the fiber samples was investigated by WAXD experiments which are performed on the undrawn fiber (DR = 1.0) as well as on fibers produced with draw ratios (DR) of DR = 5.58 and DR = 7.5. For the determination of the Hermans orientation factors, the azimuthal data of the strongest equatorial (200) reflection were analyzed for each sample. The measurements were carried out at the Institute of Crystallography of RWTH Aachen University on a STOE IPDS-II single crystal diffractometer from STOE & Cie. GmbH, Darmstadt, Germany, which is equipped with an image plate for digital readout. Molybdenum Kα-radiation with an X-ray wavelength of λ = 0.71073 Å was chosen for the experiments. The sample-detector distance was set to 200 mm, leading to a maximum observable $2\Theta_{max}$-angle of $2\Theta_{max}$ = 40°,

and the measurement time for the fiber samples was Δt = 45 min. The design of the sample holder and the principle of the fiber structure analysis have been previously reported (see [65,66] and the references therein).

2.7. Mechanical Fiber Characterization after Exposure to PBS at 37 °C

For the investigation of the mechanical properties in in vitro hydrolysis conditions, fibers with a defined length of 200 mm were fixated tension-free in rubber septa, which in turn were mounted on stainless steel rods (OK Tigrod 318SI, Esab Saldatura S.p.A, Ossona, Italy). Five fibers were attached to each rod. The sample weight in each vial was between 40 and 50 mg depending on the fiber morphology. The stainless steel rods were placed in glass vials filled with 60 mL of 9.55 g/L phosphate-buffered saline (ROTI® PreMix PBS, Carl Roth, Karlsruhe, Germany) covering the samples completely. For a sufficient buffer capacity, the PBS (pH 7.4) volume (in mL) should be at least 30 times the sample mass (in g). The samples were stored in an oven (Heraeus T12, Thermo Fisher Scientific Inc., Waltham, MA, USA) at 37 °C for 4, 8, 12 and 24 weeks, respectively. The sample size for each morphology and time of testing was n = 30 (Figure 2). Before testing, the samples were kept under standard atmosphere for textile testing according to DIN EN ISO 139 for 24 h.

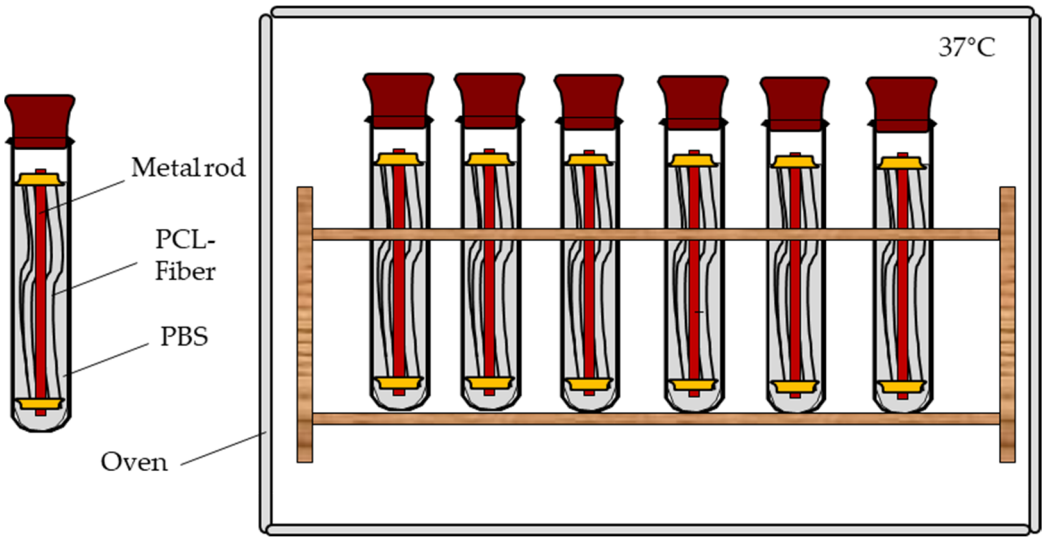

Figure 2. Polycaprolactone (PCL) fibers were fixated tension-free in glass vials. In each vial, five fibers were placed at once. The vials were filled with PBS and stored at 37 °C.

The samples were tested in a dry state by considering that (1) PCL was reported to show no difference between wet and dry testing, due to its pronounced hydrophobicity [42], (2) inaccuracies arising from slightly different exposure times to PBS (especially due to the large number of samples) can be reduced, and (3) the risk of slippage in the clamps is lowered. A universal tensile testing machine (zwickiLine Z2.5, ZwickRoell, Ulm, Germany) with a gauge length of 100 mm at a speed of 100 m/min was used. The fibers were preloaded with 0.5 cN/tex. The reference samples were prepared and tested accordingly.

2.8. Statistical Analysis

The data are displayed as the mean and standard errors of the mean (±). Statistical significance was tested using a one-sided ANOVA (analysis of variance) and was accepted if $p < 0.05$.

3. Results

3.1. Fiber Fabrication

In preliminary spinning trials, the process window of the draw ratio was investigated using a one-factor-at-a-time design. At draw ratios below 5.5, the resulted fibers were inhomogeneous in diameter, exhibiting alternating undrawn and drawn segments. Therefore, these fibers were excluded for DSC and WAXD measurements. The mechanical properties for these fibers are shown in order to illustrate the dwindling amount of undrawn segments with draw ratios approaching the natural draw ratio. The natural draw ratio (the minimal draw ratio that exhibits no undrawn segments) was identified to be approximately 5.5. At this value, a distinct and stable necking point was observed on the first godet pair (Figure 3a).

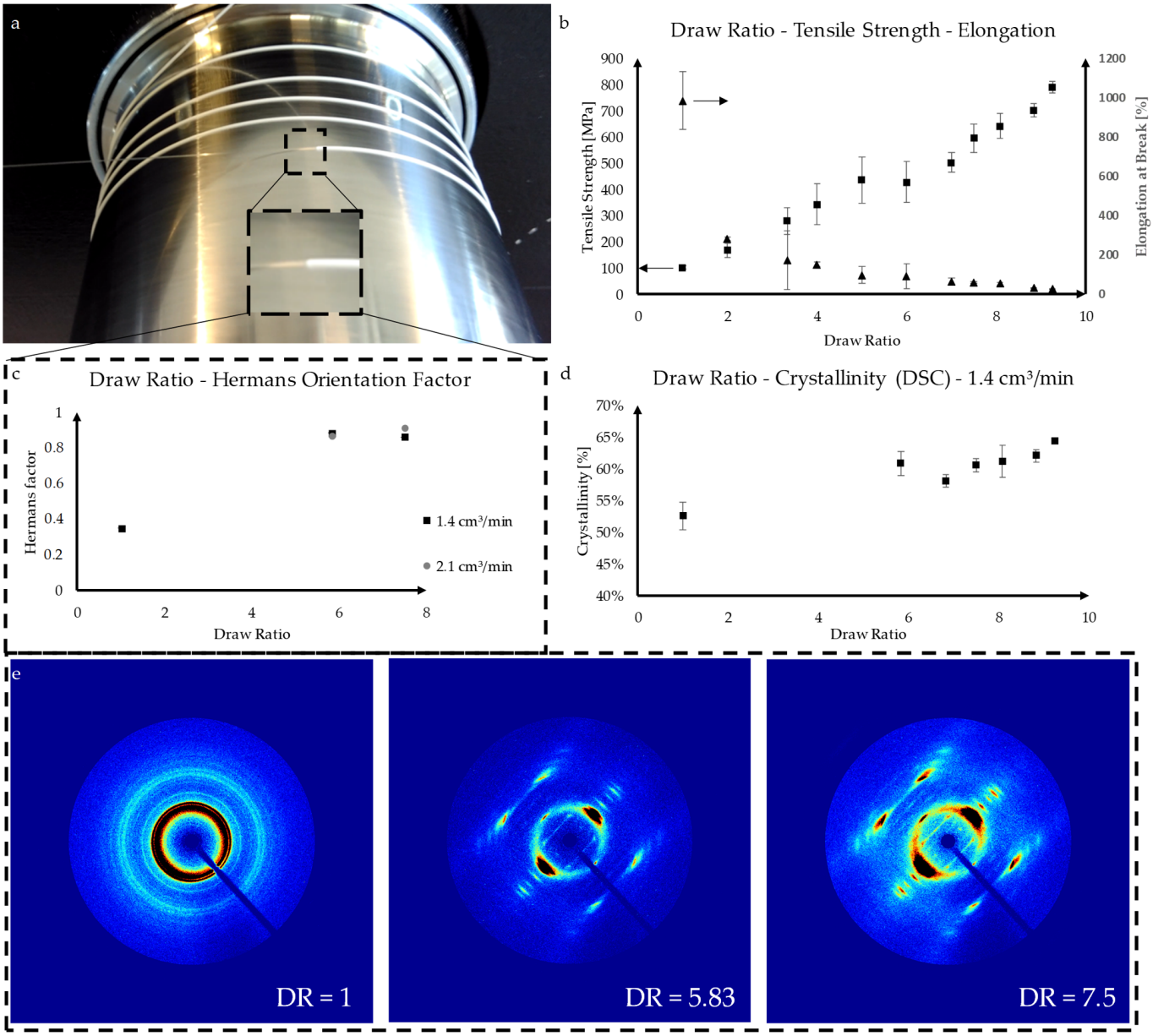

Figure 3. Influence of draw ratio (DR) on mechanical properties, orientation and crystallinity. (**a**) Locally stable and pronounced necking point during drawing between DR5.58 and DR9.25, (**b**) Effect of draw ratio on tensile strength and elongation at break, (**c**) Hermans orientation factor for a throughput of 1.4 cm^3/min and 2.1 cm^3/min, (**d**) Effect of draw ratio on crystallinity, (**e**) WAXD images for DR1, DR5.83 and DR7.5.

Compared with other thermoplastic polymers, the degree of necking is strongly pronounced for PCL. At draw ratios above 9.25, filament breakage occurred at least once each 15 min, and the rations were thus defined as unstable. The effect of the draw ratio (varied stepwise from 1 to 9.25) on the tensile strength as well as the elongation at break was investigated. As expected, the tensile strength continuously increased from 8.97 (±0.67) cN/tex at DR1 to 69.22 (±1.92) cN/tex at DR9.25, while the elongation at break asymptotically decreased from 986.33 (±147.09) % to 26.56 (±2.19) %, respectively (Figure 3b). Both effects are mainly attributed to the macromolecular orientation towards the direction of load induced in the drawing process.

The degree of orientation of undrawn fibers in contrast to fibers drawn 5.83 and 7.5 times, respectively, was investigated using WAXD. Meanwhile, an increase of the Hermans orientation factor from 0.35 for the undrawn fiber to 0.88 and 0.86 was observed for PCL_DR5.83 and PCL_DR7.5, respectively. Similar observations were made with regard to the crystallinity of the fibers. Increasing the draw ratio from 1 (undrawn) to 5.83 resulted in an increase of the crystallinity from 52.54 (±2.15) % to 60.82 (±1.86) % (Figure 3d). This phenomenon is called strain-induced crystallization. Between DR5.83 and DR7.5 (60.53 ± 1.01%) the measured crystallinity remained mostly constant before increasing again to 64.31 (±0.18) % at DR9.25.

3.2. Mechanical Fiber Characterization after Exposure to PBS at 37 °C

Besides the pure mechanical characterization of the PCL fibers, the retention of strength and elongation after different durations of exposure to PBS at 37 °C was analyzed. With respect to the application as a scaffold material, different fiber morphologies were investigated.

Fibers with modified cross-sections (Figure 4) were fabricated using different spinnerets in order to investigate potential surface-related effects on the development of the mechanical properties during a potential hydrolytic degradation induced by PBS exposure at 37 °C within 24 weeks. An overview of the fiber material used in the degradation study is displayed in Table 1.

Table 1. Overview of fibers used for exposure to PBS at 37 °C.

Sample	Shape	Yarn Structure	DR	Yarn Count [dtex]	Ref. Diameter [µm]	Max. Load [cN]	Elongation at Max. Load [%]
ROMO_5.58	Round	Monofilament	5.58	428.97	~222	1530.56	94.55
ROMU_5.58	Round	Multifilament	5.58	469.14	~76	1559.17	100.24
SFMO_5.58	Snowflake	Monofilament	5.58	452.33	~236	1624.93	88.33
SFMU_5.58	Snowflake	Multifilament	5.58	480.70	~87	1588.70	95.10

At specific times (t_1 = 4 weeks, t_2 = 8 weeks, t_3 = 12 weeks and t_4 = 24 weeks), the fibers were extracted from the PBS solution, and testing was performed on the dried fibers at a standard atmosphere for textile testing.

The different fiber morphologies are abbreviated as listed in Table 2. The development of the maximal force F_{max} and the elongation at break is illustrated in Figure 5. The outcome of the experiments reveals that a large portion of the initial maximal force is maintained during exposure to PBS. However, a distinct relation of surface morphology to the strength retention of the fibers was not observed. In contrast to other degradable synthetic polymers, which showed a certain embrittlement during the degradation process, no pronounced reduction of the elongation at break was measured for the PCL fibers.

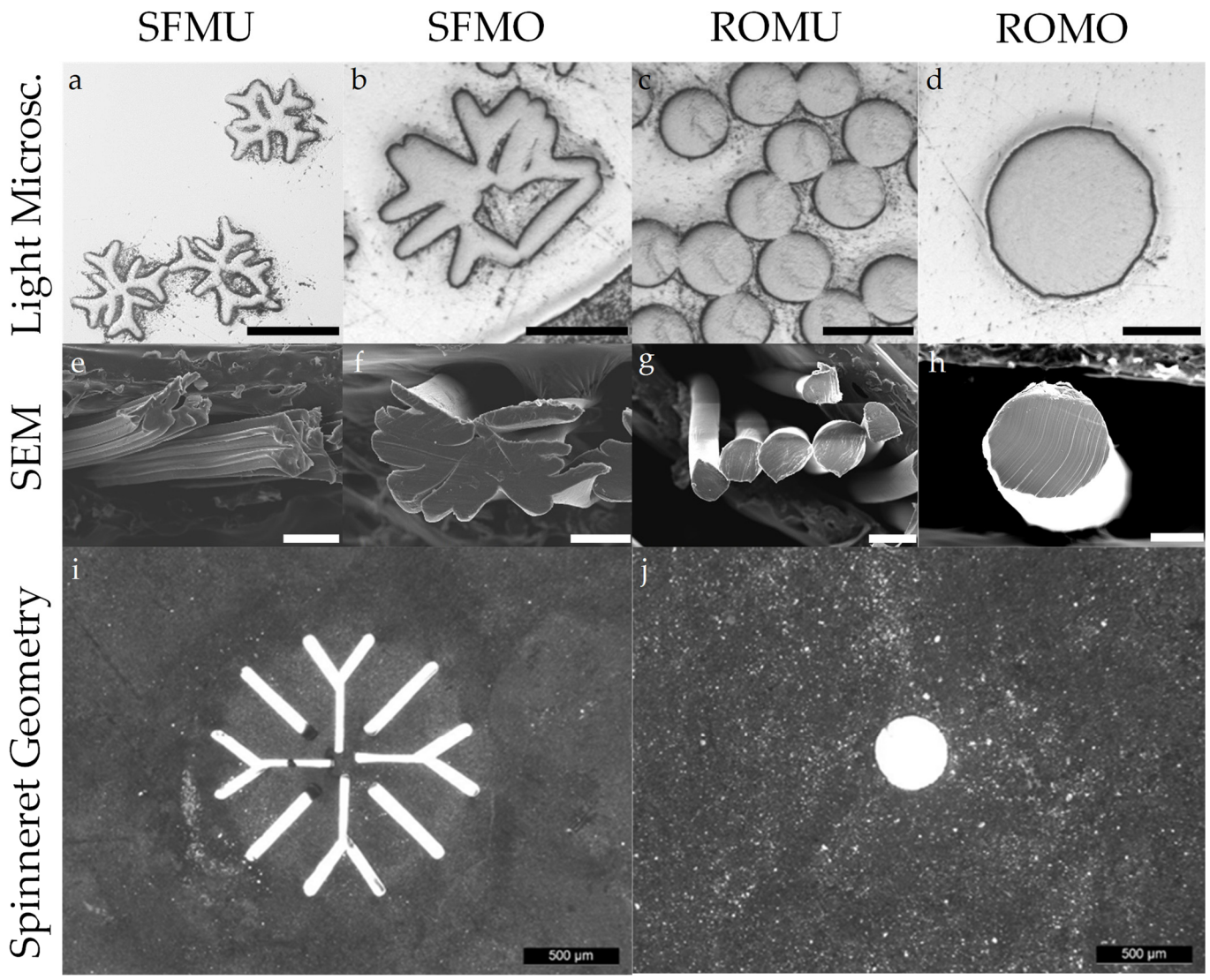

Figure 4. Optical evaluation of the melt spun PCL fibers and spinnerets used. (**a**–**d**,**i**,**j**) Light microscopy and (**e**–**h**) SEM images of the fiber cross-sections for the four different morphologies as well as (**i**,**j**) the used spinneret geometries (only monofilament spinnerets displayed). Scale bar SEM/Light Microscopy = 100 µm, Scale bar Spinneret Geometry = 500 µm.

Table 2. Fiber morphologies used for PBS exposure at 37 °C.

Full Name	Abbreviation
Round **mo**nofilament	(ROMO)
Snow**f**lake **mo**nofilament	(SFMO)
Round **mu**ltifilament	(ROMU)
Snow**f**lake **mu**ltifilament	(SFMU)

To summarize, fibers with modified cross-sections were successfully fabricated. The retention of the fibers' mechanical properties during PBS exposure at 37 °C was observed to be largely independent of the specific surface area.

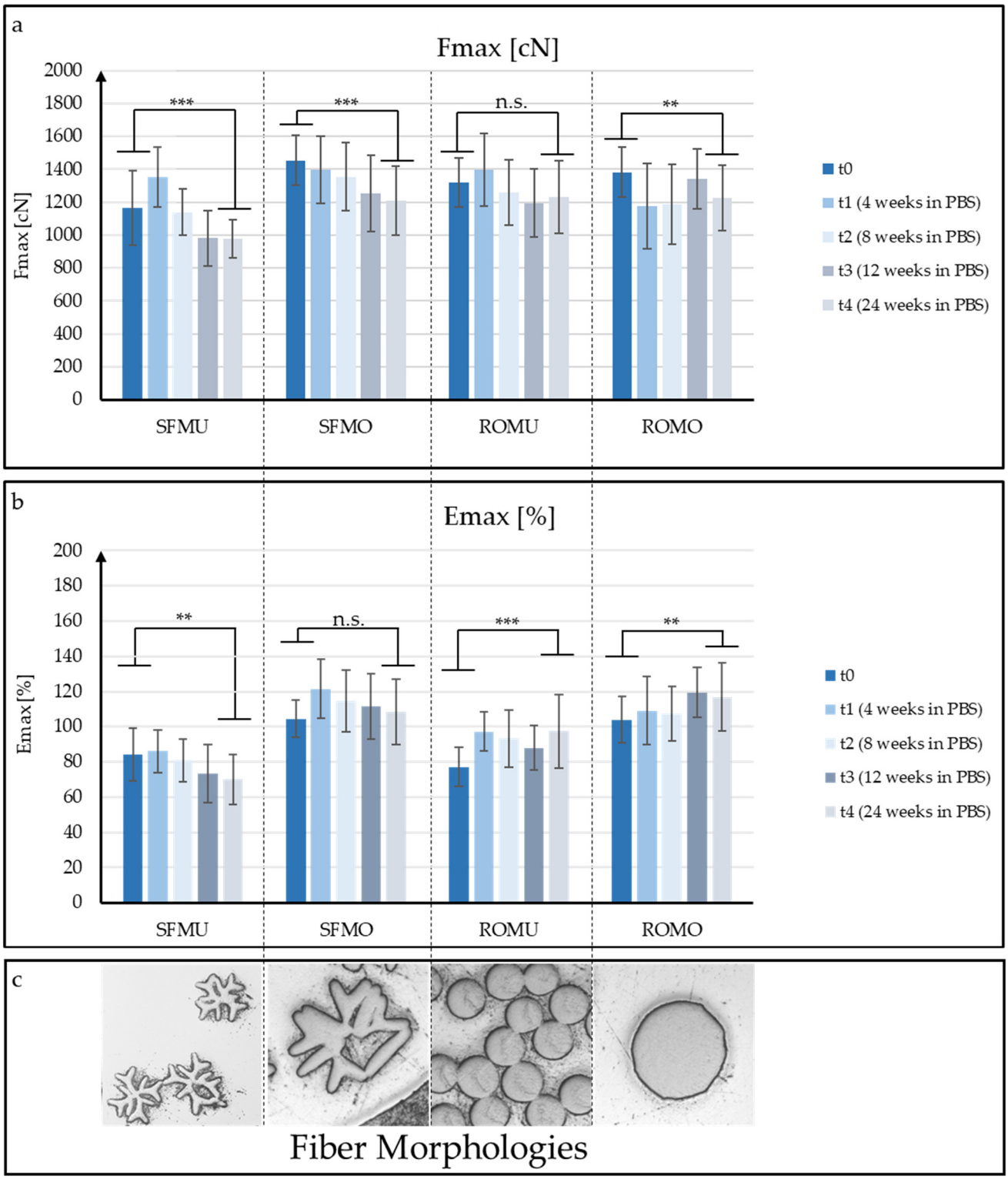

Figure 5. Mechanical fiber characterization during exposure to PBS at 37 °C for up to 24 weeks. Evaluation of max. load (**a**) and elongation at break (**b**) of melt-spun PCL fibers with different fiber morphologies (**c**). Significance levels are $p > 0.05$ (not significant), $p < 0.05$ (*), $p < 0.01$ (**), $p < 0.001$ (***). ($n = 30$, clamp sliders were excluded).

Potential changes in crystallinity during PBS exposure were investigated using DSC (Figure 6). For all fiber morphologies, an increase in crystallinity was observed, as expected (see discussion). Initially, SFMU, ROMU and SFMO exhibited a relatively homogeneous

crystallinity between 55.50 (±1.22) % and 56.09 (±1.97) %. ROMO was slightly more crystalline with 58.52 (±2.22) %. The strongest increase was measured for round multifilaments (ROMU), which reached 66.95 (±1.06) % after 24 weeks in PBS, while the lowest crystallinity was exhibited by SFMU with 61.63 (±0.58) %.

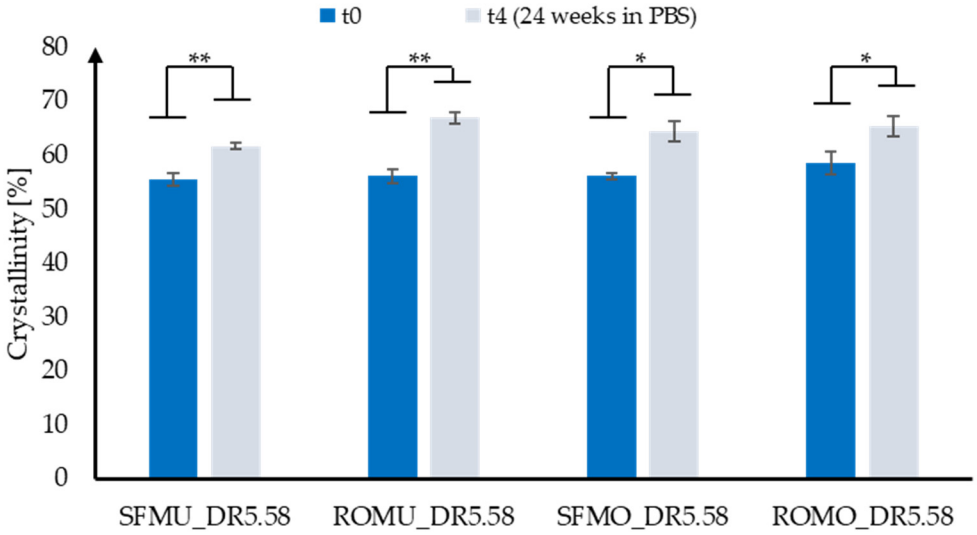

Figure 6. Crystallinity before and after 24 weeks in PBS measured for different fiber morphologies (n = 3). Significance levels are $p < 0.05$ (*), $p < 0.01$ (**).

3.3. Scaffold Production

The scaffold production was conducted using multi-layer circular braiding. Circular braiding provides good possibilities to produce different scaffold designs and to adjust the mechanical properties as well as offering an easy scalability. In a first step, the influence of the layer design for a constant number of filaments (96) on the mechanical properties and the uniformity of the structure was investigated. In a second step, a suitable layer design was selected for upscaling for a human ACL scaffold. For this part of the study, the same fiber material was used. The fibers used in this study were round monofilaments with a fineness related strength of 42.97 cN/tex (±3.84 cN/tex), an average maximum load at break of F = 15.35 N (±1.37 N) and a corresponding elongation of ε = 49.09% (±6.83%) at an average yarn count of 357.20 dtex (±0.95 dtex).

Three-layered braids with a total number of 96 filaments were produced (compare Figures 7 and 8). Meanwhile, three different layer designs were investigated. The structure *Sandwich A* consists of three layers simply braided on top of each other, while the structures *Braided Braid* and *Combination* involve the fabrication of four "pre-braids" which were subsequently processed towards the final braid. In the case of *Combination*, the outer layer was braided on top of the twice-braided core. The number of filaments n_F in each layer is illustrated (Figure 7).

During the tensile test of the braids, the following force-elongation behavior was observed. A section of lower stiffness was followed by a linear section, which was in turn followed by a plateau prior to the failure of the sample. This force-elongation behavior was attributed to a combination of structural elongation in which the fibers were oriented towards the strain axis before a linear elastic material elongation of the fibers occurred, followed by a plastic material elongation. All braids showed very reproducible loads at failure. For the first braid structure (*Sandwich A*), the maximum load at failure was F_F = 852.8 N (±18.79 N). In the *Braided Braid* structure, the first filaments broke at F_F = 850 N, and the maximum tensile force was in average F_F = 864.23 N (±11.09 N). The maximum tensile force of the third braided structure (*Combination*) was in average F_F = 855.77 N (±12.49 N). Compared to the individual fibers, the standard deviations of the

maximum load at failure were rather small, which can be attributed to a homogenization of the load distribution by fiber–fiber friction within the structure.

In summary, we observed that the maximum load of failure did not differ significantly for all braided structures ($p > 0.05$). All of these structures consisted of the same number of filaments and the same braiding angle, leading to the conclusion that the distribution of these filaments on the different layers was hardly affecting the overall load bearing of the braid within the investigated boundaries. The compactness and consequently porosity as well as tensile strength of the braid, however, are significantly determined by the layer design. These braids were elliptical in shape. Hence, the equation for ellipses was used to calculate the cross-section. Table 3 summarizes the load at failure, the ultimate tensile strength (UTS) and the cross-sections based on diameter measurements of each structure preloaded with 2 N. Due to limitations in the accuracy of the cross-section measurement, the UTS results have to be treated with caution. Nevertheless, in order to provide a rough classification of the results, the tendencies are shown below. All structures feature the appropriate tensile strength to be used as a human tendon or ligament implant (toughest ligament/tendon: Achilles tendon; ~71–86 N/mm^2 [27,67]). The produced braids in this study show a yet insufficient maximum load (primary stability), though also at much smaller cross-sections of ~7.5–9.5 mm^2, leaving room for up-scaling.

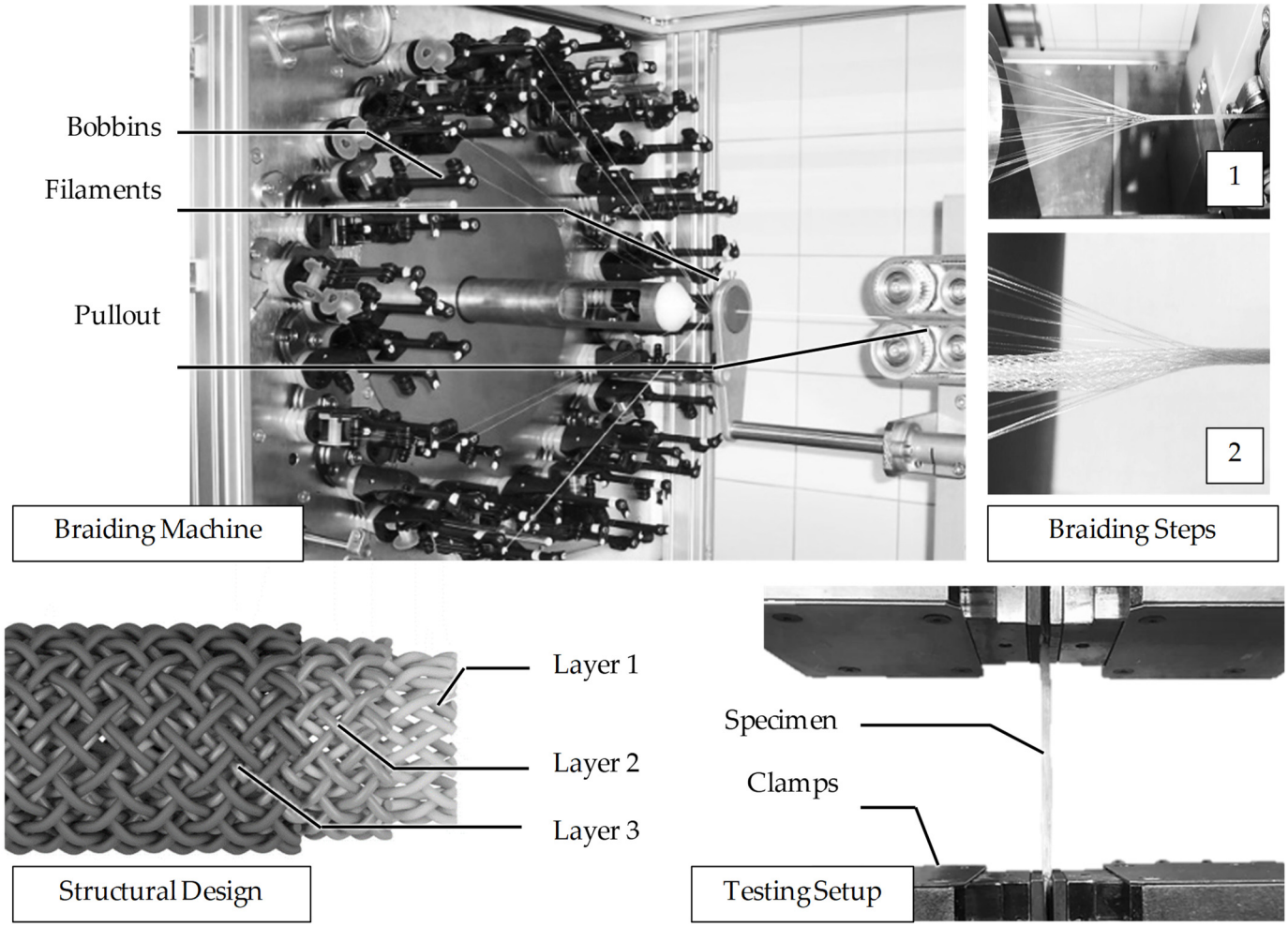

Figure 7. Multi-stage circular braiding process for scaffold production based on a three-layer design.

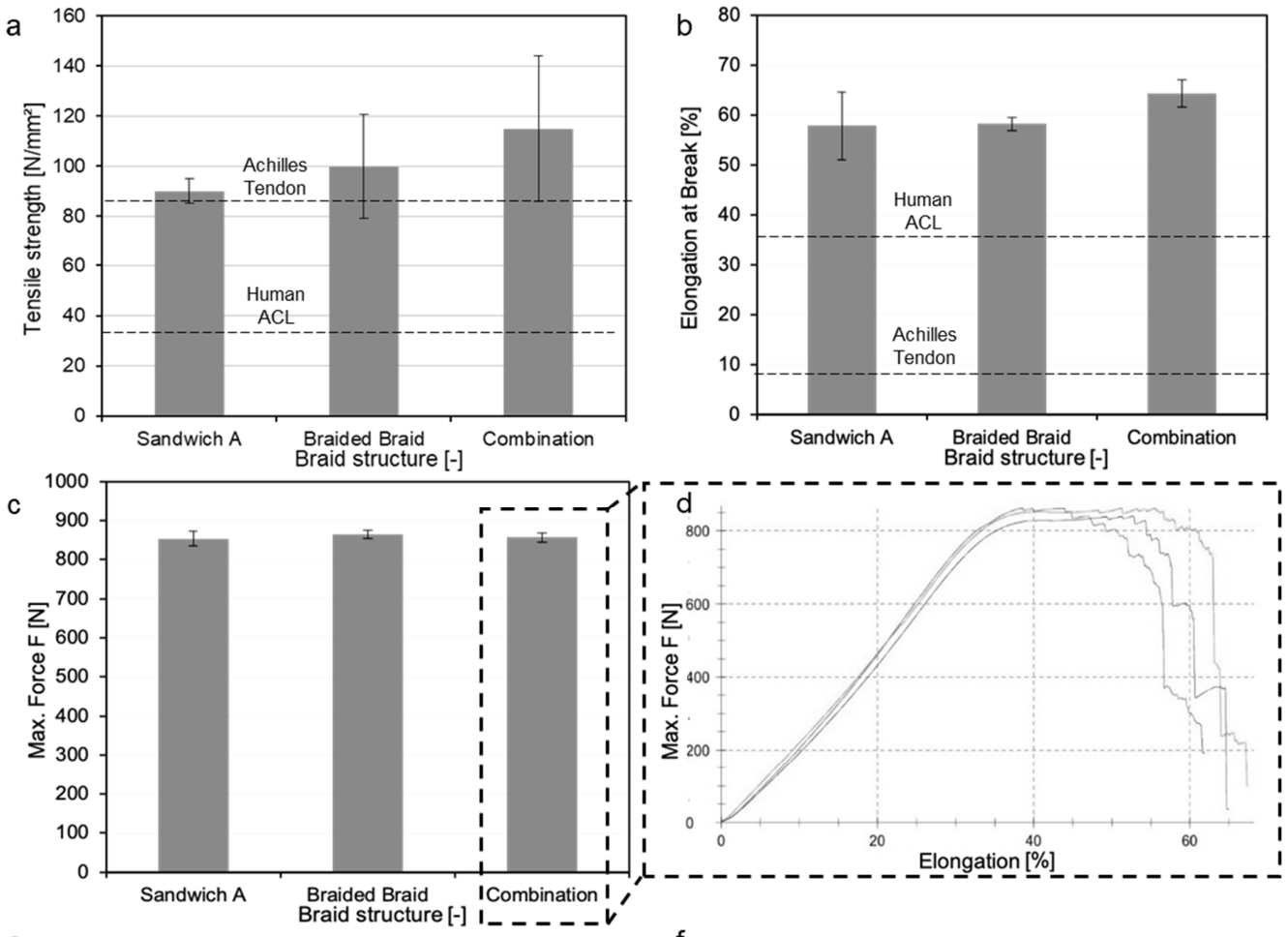

e

	Layer 1	Layer 2	Layer 3
Sandwich A	48 filaments / 13° braiding angle	24 / 13°	24 / 13°
Braided Braid	4 x 24 / 13°	4 / 13°	
Combination	4 x 12 / 13°	4 / 13°	48 / 13°

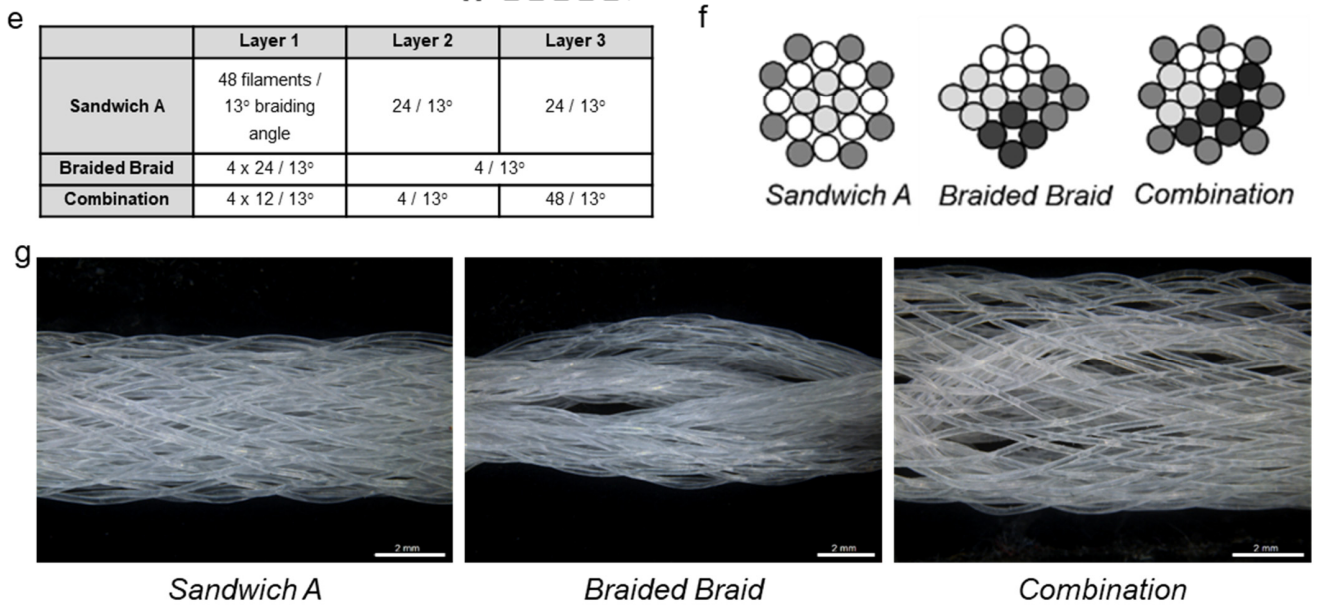

Figure 8. Mechanical characterization (n = 3) of the three braided structures (**e**–**g**—scale bar: 2 mm) comprising (**a**) tensile strength, (**b**) elongation at break and (**c**) max force. (**d**) An exemplary force-elongation-behavior is displayed for "Combination". (**e**) Filament number and braiding angle of each layer. (**f**) Schematical illustration of braided structures (different gray tones indicate subsequently braided layers (Sandwich A and Combination) or the usage of four previously braided strands (Braided Braid and Combination) and (**g**) light microscopic images of the three different braided structures.

Table 3. Comparison of different layer designs.

Layer Design (n = 3)	Load at Failure [N]	Diameter D_1 [mm]	Diameter D_2 [mm]	Cross-Section A [mm^2]	UTS [MPa]
Sandwich A	852.8 ± 18.79	4.50 ± 0.55	2.70 ± 0.26	9.47 ± 0.30	90.03 ± 4.80
Braided Braid	864.23 ± 11.09	5.29 ± 0.75	2.07 ± 0.40	8.57 ± 1.66	99.88 ± 20.77
Combination	855.77 ± 12.49	4.12 ± 0.86	2.33 ± 0.25	7.53 ± 1.81	114.84 ± 29.04

3.4. Upscaling towards Human ACL Scaffolds

In the further course of the study, the *Sandwich A* layer design was selected due to its high uniformity and scaled-up towards human ACL requirements. In order to achieve a higher load resilience, the number of filaments in the braid was doubled (2 × 96 filaments = 192 filaments), tripled (288 filaments) and quadrupled (384 filaments). The samples were abbreviated as A-96f, A-192f, A-288f as well as A-384f. The results of the follow-up tensile test (displayed in Table 4 and Figure 9) showed very low standard deviations and a nearly linear relation between the number of filaments and the resulting tensile force. A-192f exhibited a maximum load of F_{max} = 2067.38 N (±32 N) and an elongation at break of ε = 71.45% (±2%). After the force increases to the maximum at ε = 32%, it remains on a plateau until approximately ε = 60%. For A-288f, a maximum force F_{max} = 3191.03 (±60 N) was measured at ε = 30%, which remained constant until approximately ε = 60%. The highest maximum load was measured for A-384f (F_{max} = 4353.88 N (±37.3 N)), which was reached at about ε = 40%.

Table 4. Mechanical upscaling. Summary of the mechanical characteristic for varying numbers of filaments used.

Sample (n = 3)	No. of Layers	Load at Failure [N]	Diameter D_1 [mm]	Diameter D_2 [mm]	Cross-Section A [mm^2]	UTS [MPa]
A-96f	1	852.8 ± 18.79	4.50 ± 0.55	2.70 ± 0.26	9.47 ± 0.30	90.03 ± 4.80
A-192f	2	2067.38 ± 32.00	5.91 ± 0.41	4.04 ± 0.10	18.77 ± 1.59	110.14 ± 11.02
A-288f	3	3191.03 ± 60.00	9.00 ± 0.93	4.62 ± 0.95	32.30 ± 5.46	98.78 ± 18.57
A-384f	4	4353.88 ± 37.30	12.90 ± 1.87	5.35 ± 1.93	53.32 ± 16.80	81.64 ± 26.42

An important aspect of the mechanical suitability of an ACL scaffold is whether the stiffness of the scaffold can be adjusted to match the behavior of the native ACL. A stiffness that is too low would result in a loss of stability and the risk of arthritis, while an excessive stiffness may result in stress shielding [12]. The stiffness can be calculated from the slope of the linear region of the load-elongation curves. Since the stiffness is defined as force per elongation in the context of tissue-engineered ligaments, it is dependent on the gauge length of the sample. Following NF S 94-167-2, a gauge length of 100 mm was used for the tensile tests. The native ACL, however, has an approximate length of 31–38 mm [6,69].

Therefore, we calculated the equivalent stiffness for a sample length of 35 mm under the assumption that the stress–strain behavior is independent of the sample length. A potential size effect is therefore neglected. The results are displayed in Figure 10.

The calculated stiffness values of the samples A-192f, A-288f and A-384f are all within the range of the native ACL and show a nearly linear behavior with respect to the number of filaments.

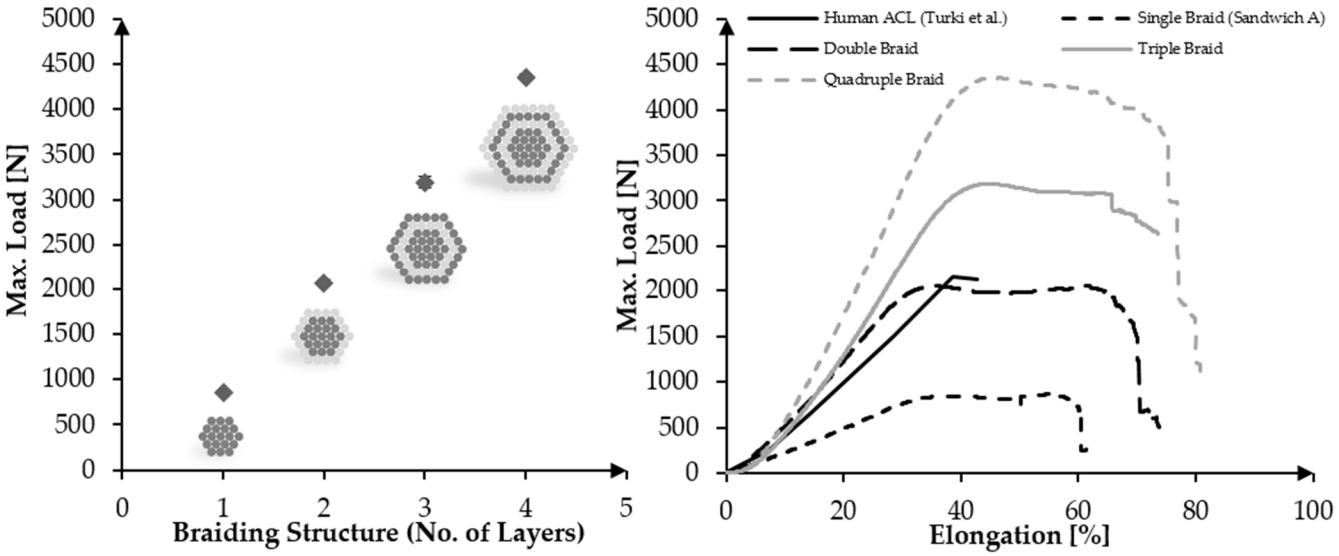

Figure 9. Upscaling of multilayer PCL braids (n = 3). (**a**) Almost linear relation of the number of layers and max. load (**b**) Force-Elongation curves of the different braids in relation to human ACL based on Turki et al. [68].

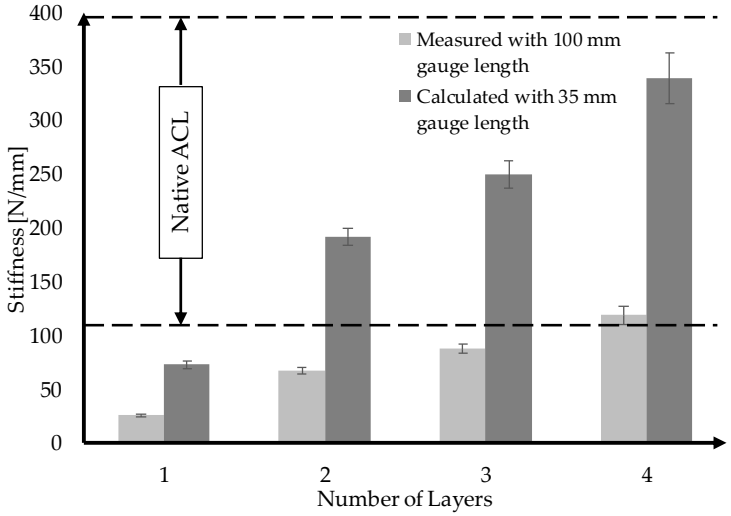

Figure 10. Stiffness derived from tensile tests (linear slope, n = 3) and calculated for an average human ACL length of 35 mm. The range of the native ACL's stiffness is indicated in dashed lines. [6].

4. Discussion

The fabrication of load-bearing, yet degradable, tissue engineering scaffolds is highly demanding. Various aspects, such as purely mechanical, process-related, degradation kinetics-related and biological requirements, need to be taken into consideration. This holds specifically true for ligament scaffolds, e.g., degradable ACL replacements. In this context, one crucial factor regarding the material choice is the mechanical long-term stability during degradation. Due to the limited intrinsic healing capacity of the respective tissue, 50% strength retention after 6 months' degradation should be aimed for [51,70]. Taking into account this limitation shortens the list of appropriate materials considerably, leaving mostly PLA and PCL as synthetic homopolymer alternatives. For PLA as well as PCL, studies report a sufficient long-term stability during degradation [51,54,55]. The potential issue of acidic degradation products of PLA, however, can be particularly problematic in

bradytrophic tissue through inflammation, on the one hand, and the risk of autocatalytic degradation and a consecutive strength loss, on the other hand. For PCL, no signs of internal catalysis were observed [22]. Leroux et al. monitored the pH value of PCL fiber bundles for 120 weeks, detecting no release of acidic species. [55]

Besides the degradation products, Fuoco et al. report a tendency of PLA to embrittlement and drastic strength loss already after 7 weeks of in vitro degradation in PBS at 37 °C. [16] In contrast to that, we did not observe a mentionable reduction of the elongation at break during PBS exposure at 37 °C for 24 weeks for PCL in the present study. Embrittlement is disadvantageous, in particular, since matching the stiffness of the scaffold with the native ACL is of huge importance for the mechanical performance.

Compared to PLA, PCL might provide higher elasticity initially as well as during degradation, which is crucial for the application as a ligament scaffold. Furthermore, a high tensile strength at relatively low stiffness can be achieved with PCL with the same scaffold structure. Aiming for the stiffness of the native human ACL which is documented between 111–396 N/mm [6,63], a higher overall breaking load can be realized with PCL, since more fibers can be used before the adequate stiffness is exceeded. PCL has been extensively investigated in the scope of tendon and ligament tissue engineering in the form of nanofibrous scaffolds [27–32,35]. For high-load applications, such as the human ACL, the rotator cuff or the Achilles tendon, a lack of scalability towards application-related strength is limiting the transferability of nanofibrous scaffolds for high-load applications. Compared with nanofibrous constructs, however, melt-spun PCL was scarcely investigated as a scaffold material for the human ACL. Leroux et al. have achieved promising biological and mechanical results using knotted melt-spun PCL fiber bundles consisting only of 20 fibers [55,61]. However, mechanical and processual feasibility is still due for a human ACL-sized scaffold.

For a complex application such as an ACL scaffold, the investigation should be conducted on the fiber level as well as on the scaffold level itself, which is to some extent intertwined, since the scaffold's properties are strongly influenced by the properties of the fibers used. On the fiber level, a sufficient tensile strength should be achieved to match the scaffold's primary stability with the demands of the native tissue (approximately 2000 N), while at the same time exhibiting sufficient porosity for cell ingrowth. Through the orientation of macromolecules induced by drawing, the tensile strength of PCL fibers was increased up to ~ 69 cN/tex. Meanwhile, a tendency to strain-induced crystallization was observed. The tensile properties of the actual fibers used in ACL scaffolds are rarely reported. Fibers produced from PLA, PLCL or PDS used for a textile-based, degradable ACL scaffold by Hahn et al. exhibited 36.12 cN/tex (PLA, 155 dtex), 35 cN/tex (PLCL, 100 dtex), 42.22 cN/tex (PLCL, 180 dtex), 30.56 cN/tex (PDS, 180 dtex) and 47 cN/tex (PDS, 100 dtex) [15,51,52]. The PLAGA multifilaments that Cooper et al. used to produce 3D-braided scaffolds showed 41.52 cN/tex (57.78 dtex) [40]. In comparison to the literature, the highly oriented PCL fibers developed in this work exhibit excellent mechanical properties and superior tensile strength.

Besides the primary stability of the fiber, its strength retention is of great importance for the regeneration of the slow healing tissue [15].

A potential means to facilitate the biological features of a scaffold on the fiber level could be the fiber morphology. For instance, earlier we reported the reduction of the scar tissue formation of sutures based on snowflake-shaped monofilaments compared to controls with a round cross-sectional morphology in an in vivo study [71].

In the present study, we compared four different fiber morphologies, all of which exhibit profoundly different specific surface areas, with respect to the mechanical properties and strength retention during exposure to PBS at 37 °C.

The average strength retention after 24 weeks in PBS (listed with increasing specific surface area) were: 88% (monofil, round), 83% (monofil, snowflake), 93% (multifil, round), 84% (multifil, snowflake). Interestingly, the results indicate no clear effect of the specific surface area (mediated through different fiber morphologies) on the strength loss. However,

snowflake-shaped fibers did in fact show a higher strength loss compared to their round counterparts. It has to be investigated in future studies whether the degradation behavior can be tailored using respective fiber morphologies.

The presented results on mechanical stability are generally in alignment with previously conducted long-term in vitro hydrolytic studies. Lam et al. even report a slight increase in tensile strength during the degradation in PBS at 37 °C for 6 months [54]. For embroidered ACL scaffolds made of PLA fibers, Hahn et al. observed a strength retention of approximately 82% after 24 weeks of hydrolytic degradation in PBS at 37 °C [51]. Leroux et al. investigated the degradation rate on PCL fiber bundles for 120 weeks in buffer saline. The development of the ultimate stress of a non-grafted PCL bundle at 37 °C indicates a reduction from ~320 MPa to ~245 MPa after 12 weeks of degradation, followed by another increase to ~310 MPa after 24 weeks [55].

The in vitro and in vivo degradation behavior of PCL has been intensively studied by Woodruff, Hutmacher et al. [22]. The degradation of PCL occurs in two stages. The first is the non-enzymatic hydrolytic degradation through chain cleavage. When the molecular weight is low enough (approximately 3000 Da), an intracellular degradation with the involvement of macrophages and giant cells was reported. [22] Hydrolytic degradation, which is dominant in the first stage, can occur either mainly via surface erosion or bulk degradation.

Whether surface erosion or bulk degradation is predominant is dependent on the water diffusion rate relative to the degradation rate and the thickness of the sample. According to Burkersroda et al. a material-specific critical length L_{crit} exists, above which the predominant degradation type is surface erosion in contrast to bulk degradation. The L_{crit} for PCL is approximately 13 mm [72]. For example, Chen et al. investigated the in vitro degradation behavior of PCL in the shape of microparticles compared to a film made of PCL, finding no obvious effect on the degradation rate [73]. Leroux et al. report similar results in a long-term in vitro degradation study of round PCL monofilament bundles in comparison with PCL films, also indicating PCL bulk hydrolysis. Hence, the degradation rate is also expected to be largely independent of the shape of the fiber (<1 mm). Our results are in alignment with this. Consequently, the fiber morphology can be utilized to add functionality in terms of cell growth guidance or to trigger surface-related effects without compromising on the mechanical strength retention.

Even though the potential of non-circular fibers can be immense, very few respective studies exist for PCL. Park et al. investigated the influence of three different fiber cross-sections (circular, triangular, cruciform) on the mechanical properties, the mass loss during degradation and the cell proliferation of PCL monofilaments [74]. Since the production process involved no means to induce macromolecular orientation, the tensile strength of the resulting fibers was quite low (approximately 12–14 MPa). Therein, circular fibers showed a slightly higher tensile strength compared with the triangular and cruciform fibers. This concurs with the investigation of Babaarslan et al. and our results [75]. Regarding the degradation behavior, Park et al. observed a clear increase in mass loss for the cruciform fibers (75% after 20 days) in comparison with the circular fibers (20%), indicating a clear relationship of the specific surface area on the degradation rate (surface erosion). However, the degradation study was performed using an accelerated setup involving NaOH, with no guarantee that the general degradation kinetic is not changed by the acceleration.

During the exposure to PBS at 37 °C, an increase of crystallinity was measured for all fiber morphologies. This effect can be explained by different degradation rates for amorphous and crystalline regions in semi-crystalline polymers, such as PCL. The amorphous regions degrade faster than the crystalline regions, resulting in an increase of the relative portion of crystalline regions, and hence of the crystallinity [54,55,76–78]. Another explanation was given by Lam et al., describing a potential recrystallization due to the increased mobility of the polymer chains mediated by the 37 °C compared to room temperature [54].

Several studies address the design of braided scaffolds for the ACL based on biodegradable fibers [11,37,38,40,41,79–81]. In our study, multilayer circular braiding was used to

fabricate ACL scaffolds. For the resulting structures, no significant effect of the layer design on the mechanical behavior could be observed, as long as the filament number and braiding angle were kept constant. The standard deviations for all samples were very low, indicating a high uniformity of the textile structure.

Using a FEM simulation, Laurent et al. showed that the number of layers increases both the stiffness and the yield load of multilayer PLCL braids [11]. These observations are in line with the experimental results of our multilayer PCL braids. The PCL braids showed linear scalability with the increase of the number of layers with respect to the maximum load and stiffness. In agreement with Laurent et al., a low braiding angle of 13° was chosen in the present study to achieve the mechanical behavior of the braided scaffold comparable to the native ACL. The influence of the scaffold parameters "number of layers" and braiding angle on the porosity of the PCL braids still needs to be considered.

Freeman et al. studied various designs based on braided, twisted, and braided-twisted fibers [37]. Comparable to the braided-braid design of the PCL braids, the scaffold was produced in two stages. Freeman's study showed a significant influence on the modulus as well as the toe region due to the twisting of the fibers and subsequent braiding. Concerning the PCL multilayer braids, there was no significant difference in load at failure, stiffness and elongation at break due to the braiding of the pre-braids. Whether there is a change in the proportion of the toe region requires further investigations. Currently, surgical cruciate ligament replacement uses a drilled tunnel in the bone of 7–9 mm, corresponding to a cross-sectional area of 38.49–63.62 mm^2 [82]. The human ACL was reported to have a cross-sectional area of 57.5 ± 16.2 mm^2 [33,62]. Comparing the mechanically up-scaled scaffolds with these dimensions, each presented braided scaffold of design Sandwich A can be used with the existing surgical method.

5. Conclusions

PCL fibers were produced via melt spinning. The influence of the draw ratio on the mechanical properties and the macromolecular orientation as well as the crystallinity of the fibers were investigated. In course of this, highly oriented PCL monofilaments were fabricated, with a strength of up to 69 cN/tex. Moreover, PCL fibers in four different morphologies (round/snowflake-shaped as monofilaments/multifilaments) were fabricated using respective spinnerets. During a 24-week exposure to PBS at 37 °C, snowflake-shaped fibers exhibited a slightly faster strength loss compared with their round counterparts but—since multifilaments did not show an accelerated strength loss in comparison with monofilaments—this cannot be attributed to the surface area itself. All fibers showed high strength retention as well as the maintenance of elongation at break as opposed to potential embrittlement. Round monofilaments were further processed into three-layered circular braids. The effect of layer design on the mechanical properties of the braids was analyzed. It became apparent that the breaking load of all textile scaffolds was significantly lower than the sum of the individual fibers' breaking load. The standard deviations also decreased significantly from fiber to textile, indicating that the load was evenly distributed throughout the textile, leading to highly reproducible results for the scaffolds. Three braided structures consisting of the same number of filaments and produced with a uniform braiding angle of 13° were compared. In terms of the load at failure, no significant difference was observed. The layer design itself appeared not to be of tremendous importance regarding the load of failure.

In a second step, the braided structure (*Sandwich A*) was up-scaled to investigate whether the necessary primary stability of a human ACL could be achieved with PCL fibers. In the meantime, braids consisting of 96, 192, 288 and 384 monofilaments have been compared, resulting in a load at failure of 893.1 N (±3 N), 2067.38 N (±32 N), 3191.03 (±60 N) and 4353.88 N (±37.3 N), respectively. The nearly linear relation between the number of fibers and the load at failure allows for great scalability of the braided PCL scaffold to match the necessary primary stability of different tissues as well as to account for individual aspects. With the general suitability in terms of primary stability and processability given,

future studies will focus on biologization and long-term stability-related aspects as well as application-specific testing.

In summary, the presented study highlights the strengths and diversity of melt-spun fibers for use in the field of ligament tissue engineering. Further processing utilizing textile production technologies, e.g., braiding, provides the material with a wide variety of application options. In particular, the observed high scalability and precise adjustability of the mechanical and morphological properties while providing sufficient strength retention make the fiber material as well as the textile processing a promising platform technology. In addition to ligaments and tendons, we therefore see enormous potential for extending this technology in the future to other load-bearing tissues, such as muscle, cartilage or bone.

Author Contributions: Concept and study design, B.B., C.E., A.I., T.G. and A.B. Acquisition and analysis of fiber and in vitro degradation study related data: B.B., L.B., R.A. and T.V. Acquisition and analysis of textile related data: L.B., F.M. and C.E. Interpretation of the data: B.B., C.E. and A.B. Drafting of the work: B.B., C.E. and A.B. Critical revision of the work for important intellectual content: all. All authors have read and agreed to the published version of the manuscript.

Funding: This research received no external funding.

Acknowledgments: We acknowledge the support of the Open Access Publishing Fund of Technical University of Darmstadt.

Conflicts of Interest: The authors declare no conflict of interest.

References

1. Bogardus, R.L.; Martin, R.J.; Richman, A.R.; Kulas, A.S. Applying the Socio-Ecological Model to barriers to implementation of ACL injury prevention programs: A systematic review. *J. Sport Health Sci.* **2019**, *8*, 8–16. [CrossRef] [PubMed]
2. Nau, T.; Teuschl, A. Regeneration of the anterior cruciate ligament: Current strategies in tissue engineering. *World J. Orthop.* **2015**, *6*, 127–136. [CrossRef] [PubMed]
3. Guidoin, M.-F.; Marois, Y.; Bejui, J.; Poddevin, N.; King, M.W.; Guidoin, R. Analysis of retrieved polymer fiber based replacements for the ACL. *Biomaterials* **2000**, *21*, 2461–2474. [CrossRef]
4. Ge, Z.; Yang, F.; Goh, J.C.H.; Ramakrishna, S.; Lee, E.H. Biomaterials and scaffolds for ligament tissue engineering. *J. Biomed. Mater. Res. A* **2006**, *77*, 639–652. [CrossRef] [PubMed]
5. Jedda, H.; Abessalem, S.B.; Sakli, F. The effect of cyclic loading on the mechanical properties of artificial ligaments. *J. Textile Institute* **2011**, *102*, 332–342. [CrossRef]
6. Vieira, A.C.; Guedes, R.M.; Marques, A.T. Development of ligament tissue biodegradable devices: A review. *J. Biomech.* **2009**, *42*, 2421–2430. [CrossRef] [PubMed]
7. Schlenker, H.-J. Tissue Engineering von Bandersatz: Einfluss Mechanischer Reize auf Humane Mesenchymale Progenitorzellen und Humane Kreuzbandzellen. Ph.D. Thesis, Universität Ulm, Ulm, Germany, 2006.
8. Silva, M.; Ferreira, F.N.; Alves, N.M.; Paiva, M.C. Biodegradable polymer nanocomposites for ligament/tendon tissue engineering. *J. Nanobiotechnol.* **2020**, *18*, 23. [CrossRef] [PubMed]
9. Altman, G.H.; Horan, R.L.; Lu, H.H.; Moreau, J.; Martin, I.; Richmond, J.C.; Kaplan, D.L. Silk matrix for tissue engineered anterior cruciate ligaments. *Biomaterials* **2002**, *23*, 4131–4141. [CrossRef]
10. Hutmacher, D.W. Scaffolds in tissue engineering bone and cartilage. *Biomaterials* **2000**, *21*, 2529–2543. [CrossRef]
11. Laurent, C.P.; Durville, D.; Mainard, D.; Ganghoffer, J.-F.; Rahouadj, R. A multilayer braided scaffold for Anterior Cruciate Ligament: Mechanical modeling at the fiber scale. *J. Mech. Behav. Biomed. Mater.* **2012**, *12*, 184–196. [CrossRef]
12. Vunjak-Novakovic, G.; Altman, G.; Horan, R.; Kaplan, D.L. Tissue engineering of ligaments. *Annu. Rev. Biomed. Eng.* **2004**, *6*, 131–156. [CrossRef] [PubMed]
13. Legnani, C.; Ventura, A.; Terzaghi, C.; Borgo, E.; Albisetti, W. Anterior cruciate ligament reconstruction with synthetic grafts. A review of literature. *Int. Orthop.* **2010**, *34*, 465–471. [CrossRef] [PubMed]
14. Zhang, X.; Wu, Y.; Pan, Z.; Sun, H.; Wang, J.; Yu, D.; Zhu, S.; Dai, J.; Chen, Y.; Tian, N.; et al. The effects of lactate and acid on articular chondrocytes function: Implications for polymeric cartilage scaffold design. *Acta Biomater.* **2016**, *42*, 329–340. [CrossRef] [PubMed]
15. Gögele, C.; Hahn, J.; Elschner, C.; Breier, A.; Schröpfer, M.; Prade, I.; Meyer, M.; Schulze-Tanzil, G. Enhanced Growth of Lapine Anterior Cruciate Ligament-Derived Fibroblasts on Scaffolds Embroidered from Poly(l-lactide-co-ε-caprolactone) and Polylactic Acid Threads Functionalized by Fluorination and Hexamethylene Diisocyanate Cross-Linked Collagen Foams. *Int. J. Mol. Sci.* **2020**, *21*, 1132. [CrossRef]
16. Fuoco, T.; Mathisen, T.; Finne-Wistrand, A. Minimizing the time gap between service lifetime and complete resorption of degradable melt-spun multifilament fibers. *Polym. Degrad. Stab.* **2019**, *163*, 43–51. [CrossRef]

17. Sahoo, S.; Ouyang, H.; Goh, J.C.-H.; Tay, T.E.; Toh, S.L. Characterization of a Novel Polymeric Scaffold for Potential Application in Tendon/Ligament Tissue Engineering. *Tissue Eng.* **2006**, *12*, 91–99. [CrossRef]
18. Mengsteab, P.Y.; Nair, L.S.; Laurencin, C.T. The past, present and future of ligament regenerative engineering. *Regen. Med.* **2016**, *11*, 871–881. [CrossRef]
19. Liu, Y.; Ramanath, H.S.; Wang, D.-A. Tendon tissue engineering using scaffold enhancing strategies. *Trends Biotechnol.* **2008**, *26*, 201–209. [CrossRef]
20. Liu, X.; Baldit, A.; de Brosses, E.; Velard, F.; Cauchois, G.; Chen, Y.; Wang, X.; de Isla, N.; Laurent, C. Characterization of Bone Marrow and Wharton's Jelly Mesenchymal Stromal Cells Response on Multilayer Braided Silk and Silk/PLCL Scaffolds for Ligament Tissue Engineering. *Polymers* **2020**, *12*, 2163. [CrossRef]
21. Zhang, P.; Han, F.; Chen, T.; Wu, Z.; Chen, S. "Swiss roll"-like bioactive hybrid scaffolds for promoting bone tissue ingrowth and tendon-bone healing after anterior cruciate ligament reconstruction. *Biomater. Sci.* **2020**, *8*, 871–883. [CrossRef] [PubMed]
22. Woodruff, M.A.; Hutmacher, D.W. The return of a forgotten polymer—Polycaprolactone in the 21st century. *Prog. Polym. Sci.* **2010**, *35*, 1217–1256. [CrossRef]
23. Leong, N.L.; Petrigliano, F.A.; McAllister, D.R. Current tissue engineering strategies in anterior cruciate ligament reconstruction. *J. Biomed. Mater. Res. A* **2014**, *102*, 1614–1624. [CrossRef] [PubMed]
24. Laurent, C.P.; Ganghoffer, J.-F.; Babin, J.; Six, J.-L.; Wang, X.; Rahouadj, R. Morphological characterization of a novel scaffold for anterior cruciate ligament tissue engineering. *J. Biomech. Eng.* **2011**, *133*, 65001. [CrossRef] [PubMed]
25. Lim, W.L.; Liau, L.L.; Ng, M.H.; Chowdhury, S.R.; Law, J.X. Current Progress in Tendon and Ligament Tissue Engineering. *Tissue Eng. Regen. Med.* **2019**, *16*, 549–571. [CrossRef]
26. Rinoldi, C.; Kijeńska-Gawrońska, E.; Khademhosseini, A.; Tamayol, A.; Swieszkowski, W. Fibrous Systems as Potential Solutions for Tendon and Ligament Repair, Healing, and Regeneration. *Adv. Healthc. Mater.* **2021**, *10*, e2001305. [CrossRef]
27. Wu, Y.; Han, Y.; Wong, Y.S.; Fuh, J.Y.H. Fibre-based scaffolding techniques for tendon tissue engineering. *J. Tissue Eng. Regen. Med.* **2018**, *12*, 1798–1821. [CrossRef]
28. Li, X.; Chen, Z.; Zhang, H.; Zhuang, Y.; Shen, H.; Chen, Y.; Zhao, Y.; Chen, B.; Xiao, Z.; Dai, J. Aligned Scaffolds with Biomolecular Gradients for Regenerative Medicine. *Polymers* **2019**, *11*, 341. [CrossRef]
29. Rothrauff, B.B.; Lauro, B.B.; Yang, G.; Debski, R.E.; Musahl, V.; Tuan, R.S. Braided and Stacked Electrospun Nanofibrous Scaffolds for Tendon and Ligament Tissue Engineering. *Tissue Eng. Part A* **2017**, *23*, 378–389. [CrossRef]
30. Orr, S.B.; Chainani, A.; Hippensteel, K.J.; Kishan, A.; Gilchrist, C.; Garrigues, N.W.; Ruch, D.S.; Guilak, F.; Little, D. Aligned multilayered electrospun scaffolds for rotator cuff tendon tissue engineering. *Acta Biomater.* **2015**, *24*, 117–126. [CrossRef]
31. Beason, D.P.; Connizzo, B.K.; Dourte, L.M.; Mauck, R.L.; Soslowsky, L.J.; Steinberg, D.R.; Bernstein, J. Fiber-aligned polymer scaffolds for rotator cuff repair in a rat model. *J. Shoulder Elbow Surg.* **2012**, *21*, 245–250. [CrossRef]
32. Willbold, E.; Wellmann, M.; Welke, B.; Angrisani, N.; Gniesmer, S.; Kampmann, A.; Hoffmann, A.; de Cassan, D.; Menzel, H.; Hoheisel, A.L.; et al. Possibilities and limitations of electrospun chitosan-coated polycaprolactone grafts for rotator cuff tear repair. *J. Tissue Eng. Regen. Med.* **2020**, *14*, 186–197. [CrossRef] [PubMed]
33. Thayer, P.S.; Goldstein, A.S. *Bio-Instructive Scaffolds for Tendon/Ligament Regeneration. Bio-Instructive Scaffolds for Musculoskeletal Tissue Engineering and Regenerative Medicine*; Elsevier: Amsterdam, The Netherlands, 2017; pp. 87–112. ISBN 9780128033944.
34. Tamayol, A.; Akbari, M.; Annabi, N.; Paul, A.; Khademhosseini, A.; Juncker, D. Fiber-based tissue engineering: Progress, challenges, and opportunities. *Biotechnol. Adv.* **2013**, *31*, 669–687. [CrossRef] [PubMed]
35. Wu, S.; Wang, Y.; Streubel, P.N.; Duan, B. Living nanofiber yarn-based woven biotextiles for tendon tissue engineering using cell tri-culture and mechanical stimulation. *Acta Biomater.* **2017**, *62*, 102–115. [CrossRef] [PubMed]
36. Li, X. *A Hybrid Graft of Silk-Based Artificial Ligament and TCP/PEEK Anchorage for ACL Reconstruction*; ETH Zurich: Zurich, Switzerland, 2013.
37. Freeman, J.W.; Woods, M.D.; Laurencin, C.T. Tissue engineering of the anterior cruciate ligament using a braid-twist scaffold design. *J. Biomech.* **2007**, *40*, 2029–2036. [CrossRef]
38. Ramakrishna, H.; Li, T.; He, T.; Temple, J.; King, M.W.; Spagnoli, A. Tissue engineering a tendon-bone junction with biodegradable braided scaffolds. *Biomater. Res.* **2019**, *23*, 11. [CrossRef]
39. Cooper, J.A.; Sahota, J.S.; Gorum, W.J.; Carter, J.; Doty, S.B.; Laurencin, C.T. Biomimetic tissue-engineered anterior cruciate ligament replacement. *Proc. Natl. Acad. Sci. USA* **2007**, *104*, 3049–3054. [CrossRef]
40. Cooper, J.A.; Lu, H.H.; Ko, F.K.; Freeman, J.W.; Laurencin, C.T. Fiber-based tissue-engineered scaffold for ligament replacement: Design considerations and in vitro evaluation. *Biomaterials* **2005**, *26*, 1523–1532. [CrossRef]
41. Lu, H.H.; Cooper, J.A.; Manuel, S.; Freeman, J.W.; Attawia, M.A.; Ko, F.K.; Laurencin, C.T. Anterior cruciate ligament regeneration using braided biodegradable scaffolds: In vitro optimization studies. *Biomaterials* **2005**, *26*, 4805–4816. [CrossRef]
42. Freeman, J.W.; Woods, M.D.; Cromer, D.A.; Ekwueme, E.C.; Andric, T.; Atiemo, E.A.; Bijoux, C.H.; Laurencin, C.T. Evaluation of a hydrogel-fiber composite for ACL tissue engineering. *J. Biomech.* **2011**, *44*, 694–699. [CrossRef]
43. Mengsteab, P.Y.; Conroy, P.; Badon, M.; Otsuka, T.; Kan, H.-M.; Vella, A.T.; Nair, L.S.; Laurencin, C.T. Evaluation of a bioengineered ACL matrix's osteointegration with BMP-2 supplementation. *PLoS ONE* **2020**, *15*, e0227181. [CrossRef]
44. Madhavarapu, S.; Rao, R.; Libring, S.; Fleisher, E.; Yankannah, Y.; Freeman, J.W. Design and characterization of three-dimensional twist-braid scaffolds for anterior cruciate ligament regeneration. *Technology* **2017**, *5*, 98–106. [CrossRef]

45. Zheng, Z.; Ran, J.; Chen, W.; Hu, Y.; Zhu, T.; Chen, X.; Yin, Z.; Heng, B.C.; Feng, G.; Le, H.; et al. Alignment of collagen fiber in knitted silk scaffold for functional massive rotator cuff repair. *Acta Biomater.* **2017**, *51*, 317–329. [CrossRef] [PubMed]
46. Ouyang, H.W.; Goh, J.C.H.; Thambyah, A.; Teoh, S.H.; Lee, E.H. Knitted poly-lactide-co-glycolide scaffold loaded with bone marrow stromal cells in repair and regeneration of rabbit Achilles tendon. *Tissue Eng.* **2003**, *9*, 431–439. [CrossRef] [PubMed]
47. Chen, J.L.; Yin, Z.; Shen, W.L.; Chen, X.; Heng, B.C.; Zou, X.H.; Ouyang, H.W. Efficacy of hESC-MSCs in knitted silk-collagen scaffold for tendon tissue engineering and their roles. *Biomaterials* **2010**, *31*, 9438–9451. [CrossRef] [PubMed]
48. Learn, G.D.; McClellan, P.E.; Knapik, D.M.; Cumsky, J.L.; Webster-Wood, V.; Anderson, J.M.; Gillespie, R.J.; Akkus, O. Woven collagen biotextiles enable mechanically functional rotator cuff tendon regeneration during repair of segmental tendon defects in vivo. *J. Biomed. Mater. Res. Part B Appl. Biomater.* **2019**, *107*, 1864–1876. [CrossRef]
49. Laranjeira, M.; Domingues, R.M.A.; Costa-Almeida, R.; Reis, R.L.; Gomes, M.E. 3D Mimicry of Native-Tissue-Fiber Architecture Guides Tendon-Derived Cells and Adipose Stem Cells into Artificial Tendon Constructs. *Small* **2017**, *13*. [CrossRef]
50. Dong, Q.; Cai, J.; Wang, H.; Chen, S.; Liu, Y.; Yao, J.; Shao, Z.; Chen, X. Artificial ligament made from silk protein/Laponite hybrid fibers. *Acta Biomater.* **2020**, *106*, 102–113. [CrossRef]
51. Hahn, J.; Breier, A.; Brünig, H.; Heinrich, G. Long-term hydrolytic degradation study on polymer-based embroidered scaffolds for ligament tissue engineering. *J. Ind. Text.* **2018**, *47*, 1305–1320. [CrossRef]
52. Hahn, J. Herstellung und Charakterisierung Gestickter Trägerstrukturen auf Basis Abbaubarer, Polymerer Fadenmaterialien für das Tissue Engineering des Vorderen Kreuzbandes. Ph.D. Thesis, Technische Universität Dresden, Dresden, Germany, 2021.
53. Pal, J.; Kankariya, N.; Sanwaria, S.; Nandan, B.; Srivastava, R.K. Control on molecular weight reduction of poly(ε-caprolactone) during melt spinning-a way to produce high strength biodegradable fibers. *Mater. Sci. Eng. C Mater. Biol. Appl.* **2013**, *33*, 4213–4220. [CrossRef]
54. Lam, C.X.F.; Hutmacher, D.W.; Schantz, J.-T.; Woodruff, M.A.; Teoh, S.H. Evaluation of polycaprolactone scaffold degradation for 6 months in vitro and in vivo. *J. Biomed. Mater. Res. A* **2009**, *90*, 906–919. [CrossRef]
55. Leroux, A.; Ngoc Nguyen, T.; Rangel, A.; Cacciapuoti, I.; Duprez, D.; Castner, D.G.; Migonney, V. Long-term hydrolytic degradation study of polycaprolactone films and fibers grafted with poly(sodium styrene sulfonate): Mechanism study and cell response. *Biointerphases* **2020**, *15*, 61006. [CrossRef] [PubMed]
56. Gurarslan, A.; Caydamli, Y.; Shen, J.; Tse, S.; Yetukuri, M.; Tonelli, A.E. Coalesced poly(ε-caprolactone) fibers are stronger. *Biomacromolecules* **2015**, *16*, 890–893. [CrossRef] [PubMed]
57. Nair, L.S.; Laurencin, C.T. Biodegradable polymers as biomaterials. *Prog. Polym. Sci.* **2007**, *32*, 762–798. [CrossRef]
58. Rohindra, D.R.; Khurma, J.R. Miscibility, melting and crystallization of poly(ε-caprolactone) and poly (vinyl formal) blend. *S. Pac. J. Nat. Appl. Sci.* **2007**, *25*, 53. [CrossRef]
59. Mochizuki, M.; Nakayama, K.; Qian, R.; Jiang, B.-Z.; Hirami, M.; Hayashi, T.; Masuda, T.; Nakajima, A. Studies on the biodegradable poly (hexano-6-lactone) fibers 1. Structure and properties of drawn poly (hexano-6-lactone) fibers (Technical Report). *Pure Appl. Chem.* **1997**, *69*, 2567–2576. [CrossRef]
60. Mochizuki, M.; Hirano, M.; Kanmuri, Y.; Kudo, K.; Tokiwa, Y. Hydrolysis of polycaprolactone fibers by lipase: Effects of draw ratio on enzymatic degradation. *J. Appl. Polym. Sci.* **1995**, *55*, 289–296. [CrossRef]
61. Leroux, A.; Maurice, E.; Viateau, V.; Migonney, V. Feasibility Study of the Elaboration of a Biodegradable and Bioactive Ligament Made of Poly(ε-caprolactone)-pNaSS Grafted Fibers for the Reconstruction of Anterior Cruciate Ligament: In Vivo Experiment. *IRBM* **2019**, *40*, 38–44. [CrossRef]
62. Noyes, F.; Grood, E. The strength of the anterior cruciate ligament in humans and Rhesus. *J. Bone Joint Surg. Am.* **1976**, *58*, 1074–1082. [CrossRef]
63. Chandrashekar, N.; Slauterbeck, J.; Hashemi, J. Sex-based differences in the anthropometric characteristics of the anterior cruciate ligament and its relation to intercondylar notch geometry: A cadaveric study. *Am. J. Sports Med.* **2005**, *33*, 1492–1498. [CrossRef]
64. Kamiya, R.; Cheeseman, B.A.; Popper, P.; Chou, T.-W. Some recent advances in the fabrication and design of three-dimensional textile preforms: A review. *Compos. Sci. Technol.* **2000**, *60*, 33–47. [CrossRef]
65. Steinmann, W.; Walter, S.; Gries, T.; Seide, G.; Roth, G. Modification of the mechanical properties of polyamide 6 multifilaments in high-speed melt spinning with nano silicates. *Text. Res. J.* **2012**, *82*, 1846–1858. [CrossRef]
66. Vad, T.; Wulfhorst, J.; Pan, T.-T.; Steinmann, W.; Dabringhaus, S.; Beckers, M.; Seide, G.; Gries, T.; Sager, W.F.C.; Heidelmann, M.; et al. Orientation of Well-Dispersed Multiwalled Carbon Nanotubes in Melt-Spun Polymer Fibers and Its Impact on the Formation of the Semicrystalline Polymer Structure: A Combined Wide-Angle X-ray Scattering and Electron Tomography Study. *Macromolecules* **2013**, *46*, 5604–5613. [CrossRef]
67. Wren, T.A.L.; Yerby, S.A.; Beaupré, G.S.; Carter, D.R. Mechanical properties of the human achilles tendon. *Clin. Biomech.* **2001**, *16*, 245–251. [CrossRef]
68. Turki, S.; Marzougui, S.; Ben Abdessalem, S. Impact of polyurethane yarns on the mechanical properties of braided artificial ligaments. *J. Text. Inst.* **2015**, *106*, 912–918. [CrossRef]
69. Karmani, S.; Ember, T. The anterior cruciate ligament—1. *Curr. Orthop.* **2003**, *17*, 369–377. [CrossRef]
70. Negahi Shirazi, A.; Chrzanowski, W.; Khademhosseini, A.; Dehghani, F. Anterior Cruciate Ligament: Structure, Injuries and Regenerative Treatments. *Adv. Exp. Med. Biol.* **2015**, *881*, 161–186. [CrossRef]

71. Eickhoff, R.M.; Bolle, T.; Kossel, K.; Heise, D.; Kroh, A.; Lambertz, A.; Blaeser, A.; Gries, T.; Jockenhoevel, S.; Neumann, U.P.; et al. Improved biocompatibility of profiled sutures through lower macrophages adhesion. *J. Biomed. Mater. Res. Part B Appl. Biomater.* **2019**, *107*, 1772–1778. [CrossRef]
72. Burkersroda, F.v.; Schedl, L.; Göpferich, A. Why degradable polymers undergo surface erosion or bulk erosion. *Biomaterials* **2002**, *23*, 4221–4231. [CrossRef]
73. Chen, D.R.; Bei, J.Z.; Wang, S.G. Polycaprolactone microparticles and their biodegradation. *Polym. Degrad. Stab.* **2000**, *67*, 455–459. [CrossRef]
74. Park, S.J.; Lee, B.-K.; Na, M.H.; Kim, D.S. Melt-spun shaped fibers with enhanced surface effects: Fiber fabrication, characterization and application to woven scaffolds. *Acta Biomater.* **2013**, *9*, 7719–7726. [CrossRef]
75. Babaarslan, O.; Hacioğullari, S.Ö. Effect of fibre cross-sectional shape on the properties of POY continuous filaments yarns. *Fibers Polym* **2013**, *14*, 146–151. [CrossRef]
76. Tsuji, H.; Mizuno, A.; Ikada, Y. Properties and morphology of poly(L-lactide). III. Effects of initial crystallinity on long-termin vitro hydrolysis of high molecular weight poly(L-lactide) film in phosphate-buffered solution. *J. Appl. Polym. Sci.* **2000**, *77*, 1452–1464. [CrossRef]
77. Gleadall, A.; Pan, J.; Atkinson, H. A simplified theory of crystallisation induced by polymer chain scissions for biodegradable polyesters. *Polym. Degrad. Stab.* **2012**, *97*, 1616–1620. [CrossRef]
78. Beslikas, T.; Gigis, I.; Goulios, V.; Christoforides, J.; Papageorgiou, G.Z.; Bikiaris, D.N. Crystallization study and comparative in vitro-in vivo hydrolysis of PLA reinforcement ligament. *Int. J. Mol. Sci.* **2011**, *12*, 6597–6618. [CrossRef]
79. Liu, X.; Laurent, C.; Du, Q.; Targa, L.; Cauchois, G.; Chen, Y.; Wang, X.; de Isla, N. Mesenchymal stem cell interacted with PLCL braided scaffold coated with poly-l-lysine/hyaluronic acid for ligament tissue engineering. *J. Biomed. Mater. Res. A* **2018**, *106*, 3042–3052. [CrossRef] [PubMed]
80. Mengsteab, P.Y.; Freeman, J.; Barajaa, M.A.; Nair, L.S.; Laurencin, C.T. Ligament Regenerative Engineering: Braiding Scalable and Tunable Bioengineered Ligaments Using a Bench-Top Braiding Machine. *Regen. Eng. Transl. Med.* **2021**, *7*, 524–532. [CrossRef] [PubMed]
81. Yu, X.; Mengsteab, P.Y.; Narayanan, G.; Nair, L.S.; Laurencin, C.T. Enhancing the Surface Properties of a Bioengineered Anterior Cruciate Ligament Matrix for Use with Point-of-Care Stem Cell Therapy. *Engineering* **2021**, *7*, 153–161. [CrossRef]
82. Kohn, D.; Rose, C. Primary stability of interference screw fixation. Influence of screw diameter and insertion torque. *Am. J. Sports Med.* **1994**, *22*, 334–338. [CrossRef]